U-type Unileg Thermoelectric Module: A Novel Structure for High-temperature Application with Long Lifespan

Xue Wang[a], Hongchao Wang[*,a], Wenbing Su[a], Tingting Chen[a], Chang Tan[a], M. A. Madre[b], A. Sotelo[§,b], Chunlei Wang[#,a]

[a] School of Physics, State Key Laboratory of Crystal Materials, Shandong University Jinan 250100, P. R. China

[b] INMA, Aragon Institute of Nanoscience and Materials (CSIC-Universidad de Zaragoza), María de Luna, 3. 50018 Zaragoza, Spain

Abstract:

Strong thermal stress caused by high temperature and difference of thermal expansion coefficient (CTE) will negatively influence the lifespan of thermoelectric modules. In this work, a new high-temperature $CaMnO_3$-based U-type unileg thermoelectric module, combining an unileg structure with pn-junction, is proposed and investigated. The novel design avoids the device failure due to different CTEs and high temperature gradients. As a result, the maximal thermal stress ($\sigma_{max,TEM}$) of 3.31GPa and fatigue life of 41686 cycles are 46% and 132% of those of traditional modules at 6W and 300K, respectively. To further relieve stress concentration, the effect of rounded corners (r_u, r_l), Ag layer thickness (H_{Ag}) and length of right legs (L_R), have been studied. It has been found that larger r_u, and r_l are suitable to relieve the local stress concentration, and the lowest $\sigma_{max,TEM}$ and highest power (P_{max}) are achieved at (r_u,r_l)=(0.1,0) and (0,0.5). Moreover, larger L_R and H_A are beneficial for mechanical properties by decreasing the peak stress and dispersing the high thermal stress regions, while module performance is improved at lower L_R and H_{Ag}. Results obtained from this U-type unileg thermoelectric module should influence and guide the design and optimization of high-temperature thermoelectric generators.

Keywords: Thermoelectric module; U-type unileg structure; finite-element simulation; thermal stress; lifespan analysis.

[*] Corresponding author: E-mail: wanghc@sdu.edu.cn (H. Wang)

[§] Corresponding author: E-mail: asotelo@unizar.es (A. Sotelo)

[#] Corresponding author: E-mail: wangcl@sdu.edu.cn (C. Wang)

1. Introduction

Renewable energy sources, and technology for their exploitation, are urgently needed due to the resources shortage, environmental deterioration, and ecological damage [1-3]. Thermoelectric power generator (TEG), as a novel energy conversion technology, can realize the direct conversion between heat and electricity [4]. In contrast to traditional waste heat recovery technologies, the TEG is advantageous because of its compactness, noiselessness, vibration-less operation, no moving mechanical components, and low ecological hazards. Thus, TEGs have been applied in micropower generators, the internet of things, automobiles, spacecrafts, *etc.*, in last decades [5-7].

The thermoelectric modules, as the main components of TEGs, are typically composed of thermoelectric legs, electrodes and ceramic substrates. Based on the Seebeck effect, thermoelectric modules can directly convert waste heat into useful electricity when a temperature difference (ΔT) is stablished across the module [8]. The theoretical conversion efficiency (η) mainly depends on ΔT and figure of merit of thermoelectric materials (ZT); it is enhanced and approaches the Carnot efficiency as ΔT increases; consequently, larger ΔT benefits to obtain higher power output. However, higher temperatures will induce larger thermal stresses within the material and among the different materials in the thermoelectric module, resulting in serious deformations, fractures and even device failure. Thus, much new designs and strategies have been proposed to solve the issue of these high stresses.

Poor contact between different materials is a crucial reason for high stress and low stability. Clin *et al.* [9] proved that the stress distribution in the thermoelectric legs was greatly affected by thermal expansion coefficient (CTE) mismatch between electrodes and thermoelectric materials. In this case, Chavez *et al.* [10] proposed a new pn-junction TEG concept. In a pn-junction TEG, as shown in **Figure 1(a)**, the metal contact and substrate on the hot side are diminished, and the electrical connection is made by a direct junction of the p- and n-type thermoelectric materials. This design completely gets rid of contact issues between metal and semiconductor on the hot side and, therefore, shows great potential for constructing reliable and

long-lifetime thermoelectric devices.

Besides, the contact issues of thermoelectric material/electrode interface, and the CTE difference between n- and p-type thermoelectric materials, are also a big challenge for low-stress design. To solve this problem, Marquesn *et al.* proposed an unileg structured module for the first time in 2007. In 2008, Lemonnier *et al.* [11] fabricated and tested a prototype of oxide thermoelectric module only composed of $Ca_{0.95}Sm_{0.05}MnO$ n-legs. The unileg structure reduces the problems associated with CTE difference between p- and n-type thermoelectric legs. As a result, this architecture contributed to good mechanical strength and increased lifespan during thermal cycling. Afterwards, an improved unileg-TEG design was proposed by Wijesekara *et al.* [12], as shown in **Figure 1(b)**. Here, the integration of electrode and conductor reduced the total number of contacts in the thermoelectric device and further decreased the thermal stress. Therefore, the unileg module with pn-junction can be considered as a promising structure for low-stress design [13].

As mentioned above, the high stress intensity can be effectively reduced through novel structural design. However, for any structure, the stress at the local structure such as the edge of a hole, or at a right-angle beam, has a higher value than the remote stress [14, 15]. The phenomenon of stress concentration will result in fatigue cracks and the failure of an object or component. In this case, Al-Merbati *et al.* [16] proposed that thermal efficiency is improved for certain geometric configuration of the device. Yilbas *et al.* [17] investigated the impact of tapered and rectangular pin configurations on thermal stress in thermoelectric generators, and found that thermal stress developed in tapered configuration attains lower values than that of rectangular cross-section. Wang *et al.* [18] focused on studying the feasibility of an X-type thermoelectric module with different draft angles. They found that the X-type structure can enhance the performance of the thermoelectric module with regard to both electrical power and mechanical reliability. The effect of soldering thickness has been researched by Wu *et al.* [19], and they proposed choosing a suitable tin soldering thickness will not only alleviate thermal stress intensity in the module, but also increases thermal efficiency. All in all, unreasonable geometric structure is a main

reason for high local stress, which will degrade the module performance and lifespan [20-22]. Geometry optimization, such as rounded or chamfered corners and conductor with optimal thickness, is a good method to solve problems of stress concentration.

In this work, an U-type unileg thermoelectric generator, combining an unileg structure with pn-junction, is proposed and investigated to relieve the crucial problem of high thermal stress and short lifespan caused by CTE difference or high heat flux. Moreover, the geometric parameters, such as rounded corners (r_u, r_l), thickness of Ag layer (H_{Ag}), and length of right legs (L_R), are optimized to further relieve stress concentration. The results showed that the U-type unileg thermoelectric module has excellent mechanical strength and long lifespan, which would be highly beneficial for commercializing high-temperature thermoelectric devices.

2. Simulation approach

2.1 Numerical model

The schematic diagram of the U-type unileg thermoelectric module with r_u=r_l=0mm, as an example, is constructed and drawn by COMSOL and SOLIDWORKS in **Figure 1(c)**. The designed thermoelectric module is assembled with Al_2O_3 plates, Ag electrodes, and Dy-doped $CaMnO_3$ unileg with an Ag-coated side. The dimensions ($l_x \times l_x \times l_z$) of upper and lower Al_2O_3 plates are $17\times2\times0.1mm^3$ and $19\times2\times0.1mm^3$, respectively. The electrodes, with $5\times2\times0.027mm^3$ size are used to connect the unilegs and Al_2O_3 plates, while the terminal electrodes with $0.027\times2\times1mm^3$ size, are applied to connect load resistance. This Ag-coated unileg design is the main part of the U-type module studied in this work. Here, three interconnected thermoelectric unilegs are obtained from a single block of material. The spacing between adjacent thermoelectric materials are alternatively connected to the upper or lower substrate, having $1\times2\times4.027mm^3$ dimensions. The Ag-coating layer, with 35μm thickness, is deposited on the right side of each unileg, and the junction region between two unilegs, which is used for electric conduction. In other words, three left thermoelectric legs are connected through Ag-coated right legs electrically in series. The thickness of electrode and Ag-coating layer are chosen from previously reported experimental articles [7, 23]. The

temperature-dependent thermoelectric properties of Dy-doped $CaMnO_3$ are shown in **Figure S1** [24]. The density (ρ_d), Young's modulus (E), Poisson's rate (v), and CTE, of Dy-doped $CaMnO_3$ (CMO-Dy), Ag and Al_2O_3 are presented in **Table S1**.

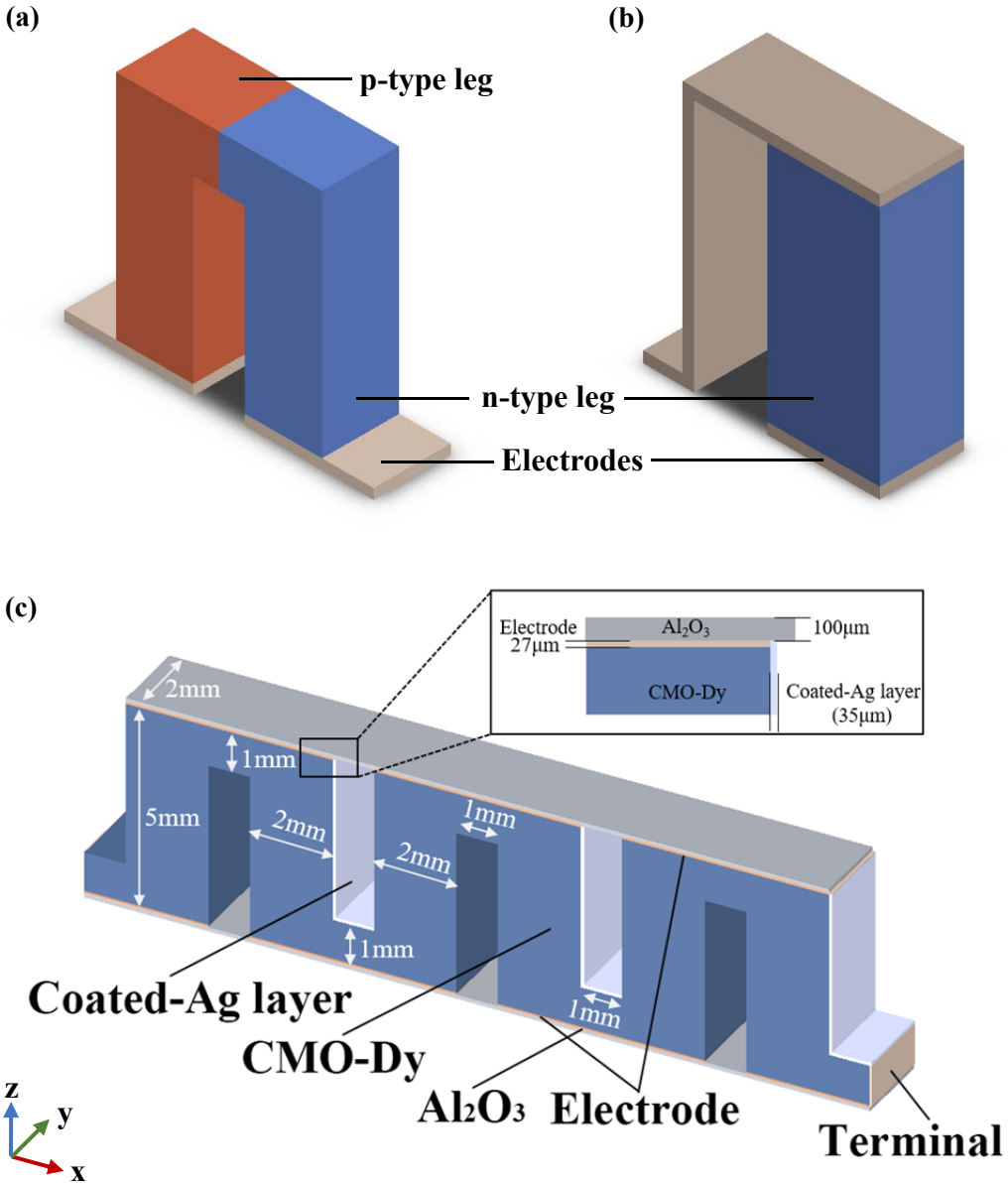

Figure 1 The schematics of (a) a π-type thermoelectric module with pn-junction; (b) a unileg thermoelectric module; and (c) a U-type unileg thermoelectric module with straight corners.

2.2 Finite-element simulation

Stablishing the relationship between module design and physical properties is the main objective in the simulation. Some boundary conditions and reasonable assumptions are adopted for this purpose. Firstly, the thermoelectric module is in

steady state. Secondly, the thermoelectric module is regarded as an adiabatic system where the heat radiation and convection on all surfaces, except on the hot and cold ends, are ignored. Thirdly, the upper and lower sides of module are considered as the hot and cold ends. The absorbed heat in the hot side (Q_h) is assumed to be constant, 6W, and the cold-end temperature is fixed at 300K. Fourthly, the electrical and thermal contacts between thermoelectric materials and Ag-coating layer, or Ag electrodes, are considered [25]. The surface roughness and surface roughness slope are, respectively, 0.08μm and 0.544, according to previously reported experimental results [26]. Fifthly, the leftmost electrode is grounded, and rightmost electrode is terminal. Sixthly, the bottom of the U-type unileg module is fixed.

The heat flux and electric current coupled phenomena in the thermoelectric module can be well calculated and analyzed through the governing equations shown below [27, 28].

$$\nabla \cdot \boldsymbol{q} = \boldsymbol{J}^2/\sigma \quad (1)$$

$$\nabla \cdot \boldsymbol{J} = 0 \quad (2)$$

In here, $\boldsymbol{J}^2/\sigma$ is the term of Joule heat. The heat flux vector ($\boldsymbol{q}$) and current density vector ($\boldsymbol{J}$) in three dimensions can be calculated as follows.

$$\boldsymbol{q} = -\kappa(T)\nabla T + P_c(T)\boldsymbol{J} \quad (3)$$

$$\boldsymbol{J} = -\nabla V/\rho(T) + S\nabla T/\rho(T) \quad (4)$$

where $S(T)$, $\rho(T)$, $\kappa(T)$ and $P_c(T)$ are the temperature-dependent Seebeck coefficient, electrical resistivity, thermal conductivity, and Peltier coefficient calculated by $S(T)T$, respectively. ∇T and ∇V are the temperature and electric potential gradients. Based on the above equations, the thermoelectric constitutive equations can be described by Equations (5) and (6),

$$\nabla \cdot (\kappa(T)\nabla T) + \rho(T)\boldsymbol{J}^2 - T\boldsymbol{J}((\partial S/\partial T)\nabla T + \nabla S) = 0 \quad (5)$$

$$\nabla \cdot (-(\nabla V + S(T)\nabla T)/\rho(T)) = 0 \quad (6)$$

Based on simulative results, the module performance results include internal resistance (R_{in}), output voltage (V_o), working current (I), output power (P), and maximum output power (P_{max}), which are calculated through the following expressions.

$$R_{in} = \int \rho_d(T)\mathrm{d}l/\mathrm{d}S, \quad T = f(x, y, z) \quad (7)$$

$$V_o=(R_L/(R_{in}+R_{load}))\int S(T)\mathrm{d}T \quad (8)$$

$$I=V_o/R_L=\int S(T)\mathrm{d}T/(R_{in}+R_{load}) \quad (9)$$

$$P=I^2R_L=(\int S(T)\mathrm{d}T)^2/(R_{in}+R_{load}) \quad (10)$$

$$P_{max}=(\int S(T)\mathrm{d}T)^2/4R_{in} \quad (11)$$

Here, R_{in} depends on the temperature field and current direction; dl and dS are unit length along the current direction, and unit cross-sectional area perpendicular to the current direction, respectively; R_L is the load resistance.

Thermal stress is generated due to the differential thermal expansion of materials forming the thermoelectric generator. The equations governing the displacement-strain relations for the thermal stress can be expressed as shown below [16, 29].

$$\bar{\varepsilon}_{xx}=\frac{\partial\bar{u}}{\partial\bar{x}},\ \bar{\varepsilon}_{yy}=\frac{\partial\bar{v}}{\partial\bar{y}},\ \bar{\varepsilon}_{zz}=\frac{\partial\bar{w}}{\partial z} \quad (12)$$

$$\bar{\varepsilon}_{xy}=0.5(\frac{\partial\bar{u}}{\partial\bar{y}}+\frac{\partial\bar{v}}{\partial\bar{x}}),\ \bar{\varepsilon}_{yz}=0.5(\frac{\partial\bar{w}}{\partial\bar{y}}+\frac{\partial\bar{v}}{\partial\bar{z}}),\ \bar{\varepsilon}_{zx}=0.5(\frac{\partial\bar{w}}{\partial x}+\frac{\partial\bar{u}}{\partial z}) \quad (13)$$

The stress-strain relation can be expressed in a dimensionless form using a nonsymmetrical Jacobian matrix

$$\begin{Bmatrix}\bar{\sigma}_{xx}\\ \bar{\sigma}_{yy}\\ \bar{\sigma}_{zz}\\ \bar{\sigma}_{yz}\\ \bar{\sigma}_{zx}\\ \bar{\sigma}_{xy}\end{Bmatrix}=\frac{\bar{E}}{(1+v)(1-2v)}\begin{bmatrix}1-v & v & v & 0 & 0 & 0\\ v & 1-v & v & 0 & 0 & 0\\ v & v & 1-v & 0 & 0 & 0\\ 0 & 0 & 0 & 1-2v & 0 & 0\\ 0 & 0 & 0 & 0 & 1-2v & 0\\ 0 & 0 & 0 & 0 & 0 & 1-2v\end{bmatrix}\times$$

$$\begin{Bmatrix}\bar{\varepsilon}_{xx}\\ \bar{\varepsilon}_{yy}\\ \bar{\varepsilon}_{zz}\\ \bar{\varepsilon}_{yz}\\ \bar{\varepsilon}_{zx}\\ \bar{\varepsilon}_{xy}\end{Bmatrix}-\begin{Bmatrix}1\\1\\1\\0\\0\\0\end{Bmatrix}\frac{\overline{\alpha ET}}{1-2v} \quad (14)$$

The three principal stresses are represented as σ_1, σ_2, and σ_3, respectively. The von Mises equivalent stress can be obtained from the fourth strength theory of mechanics of materials also known as the distortion of energy theory. It describes the total combined stresses in all three dimensions,

$$\sigma=\sqrt{\frac{[(\sigma_1-\sigma_2)^2+(\sigma_2-\sigma_3)^2+(\sigma_3-\sigma_1)^2]}{2}} \quad (15)$$

The fatigue limit can be provided by a combined Basquin and Coffin-Manson relation

[30-32], given by

$$\varepsilon_{\mathrm{a}} = \frac{\sigma_{\mathrm{f}}'}{E}(2N_{\mathrm{f}})^{b} + \varepsilon_{\mathrm{f}}'(2N_{\mathrm{f}})^{c} \quad (16)$$

where σ'_{f} is the fatigue strength coefficient, b is the fatigue strength exponent, $\varepsilon'_{\mathrm{f}}$ is the fatigue ductility coefficient, c is the fatigue ductility exponent, and E is the Young's modulus. N_{f} is the number of load reversals, and thus $2N_{\mathrm{f}}$ is the number of full cycles to failure, N, at a strain amplitude of ε_{a}. At low strains the fatigue life is limited by a Cycle Cutoff. It is well known that the mean stress has a significant effect on the fatigue life. Morrow proposed a mean stress correction to the Basquin part of the combined Basquin and Coffin-Manson relation according to

$$\varepsilon_{\mathrm{a}} = \frac{\sigma_{\mathrm{f}}' - \sigma_{\mathrm{ave}}}{E}(2N_{\mathrm{f}})^{b} + \varepsilon_{\mathrm{f}}'(2N_{\mathrm{f}})^{c} \quad (17)$$

where σ_{ave} is the mean stress of the load cycle.

2.3 Model validation

To verify the correctness of the simulation method, an experimental $GdCo_{0.95}Ni_{0.05}O_{3-\delta}/CaMn_{0.98}Nb_{0.02}O_{3-\delta}$ thermoelectric module is simulated and analyzed by the above same mathematical model at ΔT of 500K [33]. In addition, the distribution of von Mises stress for a π-type thermoelectric module studied by Karri *et al*. is also simulated and analyzed at T_{h}=250°C and T_{c}=100°C [34]. When comparing these results to the simulated ones, presented in **Figures S2** and **S3**, the distributions of R_{in}, open-circluit voltage (V_{oc}), P_{max} and maximum von Mises stress (σ_{max}), are well matched with those obtained in reference. The deviations between experimental and simulated values on R_{in}, V_{oc}, P_{max} and σ_{max} are only 1.62%, 2.86%, 7.42% and 8%, respectively. The deviation is owing to the difference of some initial setting values, which are not described in the reference. Anyway, the main factors and effects have been considered in this simulation work, so the simulated results obtained in this work are credible.

2.4 Mesh convergence

Mesh convergence test has been performed to raise confidence in the simulative results of the U-type unileg module. As a result, the average hot-side temperature ($T_{h\text{-}ave}$) and P_{max} of four meshes consisting of 12800, 42465, 85980, and 108005 cells, are 859.74, 859.76, 859.80, and 859.80K; and 6.613, 6.614, 6.616, and 6.616mW, respectively. Thus, the model with 85980 cells exhibits the best balance in terms of accuracy and computational time, and has been selected for the following simulation.

3. The performance of the U-type unileg module

Figure 2 shows the temperature and voltage distribution of the U-type unileg module without rounded corners at Q_h=6W and T_c=300K under open-circuit conditions. As presented in **Figure 2(a)**, the temperature fluctuates up and down along x-axis, while maintained unchanged along y-axis, and monotonously increased along z-axis. It means that the heat flux flow from the hot-side substrate to the left legs and Ag-coated right legs, and then to the lower electrodes and cold-side substrate. To gather more detailed information about the hot-side temperature distribution, the evolution of temperature for the thermoelectric unileg/electrode interface ($T_{TEU/E}$), electrode/Al_2O_3 interface ($T_{E/A}$), and upper side of Al_2O_3 plate (T_h) along x-axis (black line in **Figure 2(a)**), are exhibited in **Figure 2(c)**. The $T_{E/A}$, and T_h curves are well coincident due to the high thermal conductivity of Al_2O_3 plate. The temperature drops in the unileg region (x=0-5mm, 6-11mm, 12-17mm), and then rapidly increases in the junction region between different unilegs (x=5-6mm, 11-12mm). The abrupt change of temperature is caused by the high thermal conductivity of Ag-coating layer and large concentrated heat flux in the junction region. Consequently, the maximum hot-side temperature ($T_{h,max}$) of 905.25K and minimum value ($T_{h,min}$) of 769.94K are obtained at leftmost and rightmost sides of the upper Al_2O_3 plate, respectively, leading to 861.15K average value ($T_{h,ave}$). The variation tendency of $T_{TEU/E}$ for the three unilegs are similar. The temperature, as actual hot-side temperature of thermoelectric material, in the unileg region is firstly raised, followed by dropping along the x-axis direction, and then showing a sharp increase at the Ag-coating layer position. The peak value

appears at the middle of the unileg region because of the high concentrated heat flux. In addition, the temperature variation curves of left and right legs, for leftmost unileg, along z-axis are presented in **Figure 2(d)**, where the bottom side of the module is set as z=0mm. In this figure, the temperature of both legs goes up as height increases. However, the actual temperature differences (ΔT_a) of left and right legs are 450.98, and 410.15K, respectively, which are much lower than the ΔT across the module, 561.15K, (ΔT=$T_{h,ave}$-300K).

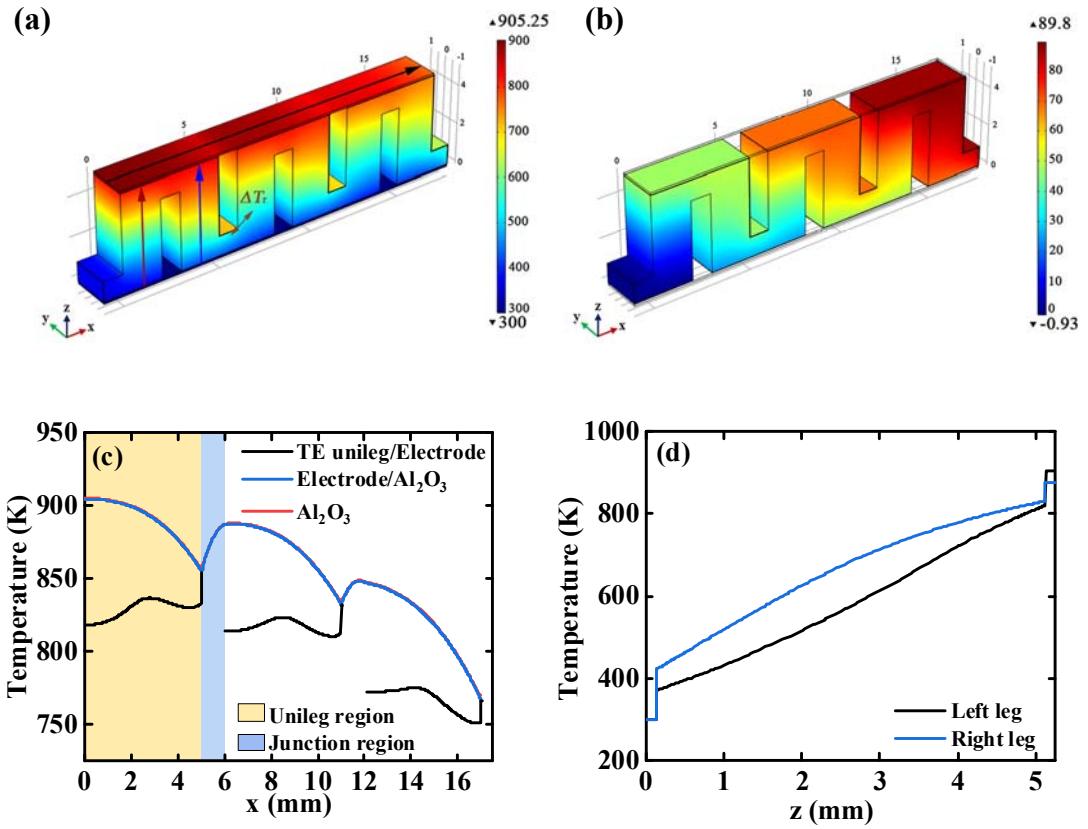

Figure 2 The (a) temperature; and (b) voltage distributions of for the U-type unileg module under open-circuit conditions. (c) Temperature variation of thermoelectric unileg/electrode interface, electrode/Al_2O_3 interface, and Al_2O_3 surface along x-axis. (d) Temperature variation of left and right legs for leftmost unileg along z-axis.

These lower ΔT_a values are mainly due to the high thermal contact resistance between electrode and thermoelectric materials. Moreover, the larger ΔT_a of left leg compared to the right one is owing to the relatively lower thermal resistance (R_{th}) of right leg with Ag-coating layer. Based on the temperature distribution above mentioned, the voltage distribution of the U-type unileg module in open-circuit condition is described

in **Figure 2(b)**. In this figure, the right legs are practically short-circuited and act as electrical conductors in the unileg structure; in other words, the left legs of three unilegs are electrically connected in series through right legs with Ag-coating layer. Consequently, the module will keep working even if the electrode and Al_2O_3 in the hot side are broken. Furthermore, the V_{oc} does not monotonically increase because the reverse temperature difference (ΔT_r) between junction region and the left leg of the adjacent unileg results in voltage losses. Finally, the V_{oc} generated by these three unilegs is 89.8mV at Q_h=6W, with $T_{h,ave}$=861.15K and T_c=300K.

Figure 3(a) plots the distribution of von Mises stress when the bottom of the module is fixed. Obviously, the stress distribution in the unileg module is inhomogeneous due to the complex geometric structure and temperature field. However, most area is subjected at low σ (<0.5GPa), as shown in **Figure 3(b)**, while the high stresses are locally presented at the hot-side ceramic substrate (**Figure 3(c)**), and the right-angle corners (**Figure 3(d)**). More specifically, the variation of σ for the unileg/electrode interface ($\sigma_{TEU/E}$), electrode/Al_2O_3 interface ($\sigma_{E/A}$) and Al_2O_3 surface (σ_A) along x-axis are shown in **Figure 3(e)**. The maximum stress (3.31GPa) is obtained at the Ag-coating layer position (x=5mm), in the electrode/Al_2O_3 interface, which is the most likely place for a crack. Considering the free expansion along y-axis and the rigid joints along x- and z-axis, the crack will develop along y-axis.

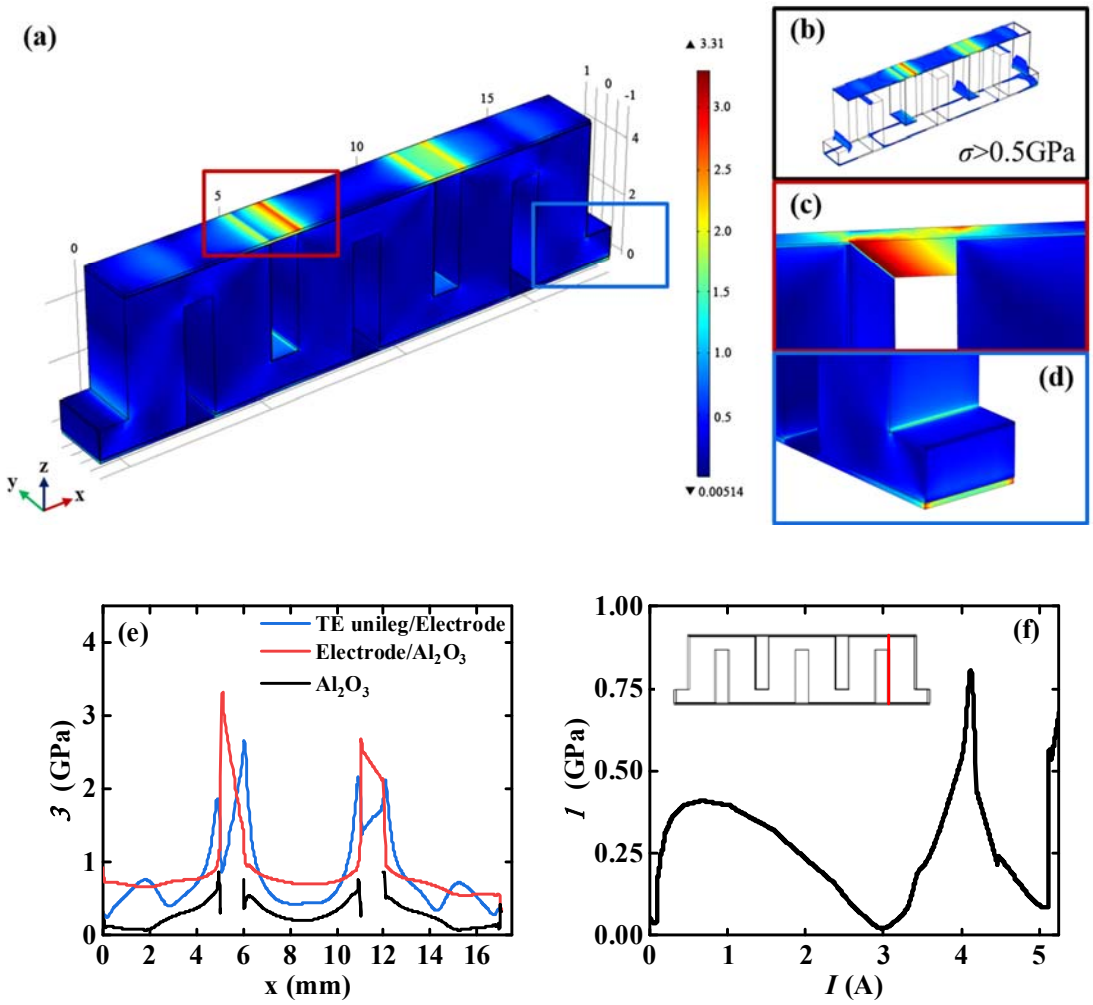

Figure 3 (a-d) von Mises stress distribution of the U-type unileg module under open-circuit conditions. (e) Variation of von Mises stresses for the unileg/electrode interface, electrode/Al_2O_3 interface and Al_2O_3 surface along x-axis. (f) Variation of von Mises stress along z-axis.

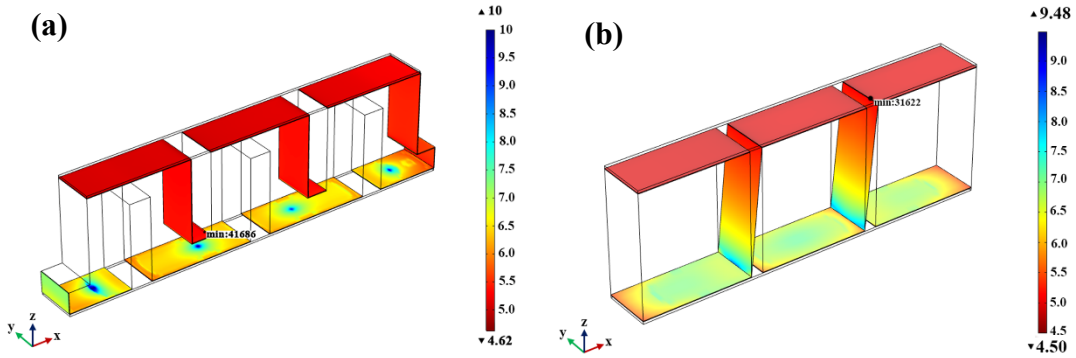

Figure 4 The fatigue life of (a) U-type unileg module; and (b) traditional unileg module.

For $\sigma_{TEU/E}$ and σ_A, the highest stress values are obtained at x=5, 6, 11, and 12mm. The phenomenon of stress concentration is caused by the coupled effect of large temperature gradients, right-angle structure, and CTE difference between Ag electrodes and Al_2O_3 substrate. In addition, the variation of σ along z-axis (red line in the illustration) is presented in **Figure 3(f)**, when the bottom side of the module is z=0mm. The σ rises and falls repeatedly as increasing height. The first peak value, 0.41GPa, occurs at z=0.6mm due to the strong constraint caused by the surrounding material; the second peak value, 0.95GPa as the maximum value, is obtained at z=4.1mm, because of the right-angle structure; and the third peak value, 0.67GPa, emerges on the upper side of the module owing to the high temperature and CTE difference. Compared to the traditional unileg module, as presented in **Figure S4**, the σ_{max} for both modules are obtained at junction regions of hot end. The σ_{max} of the overall thermoelectric module ($\sigma_{max,TEM}$), TE materials ($\sigma_{max,TE}$) and electrode ($\sigma_{max,E}$) for traditional unileg module are 7.15, 1.65 and 4.26GPa, which are 116%, 3.8% and 78.2% higher than the obtained for the U-type unileg module, respectively.

Figure 4 presents the fatigue life of the electrode and Ag-coating layer for U-type unileg module and traditional unileg module to better reflect the module stability. The fatigue life is calculated by formulas 16 and 17 based on the combined Basquin and Coffin-Manson model. Here, σ'_f, ε'_f, b, and c of Ag are set as 44.5MPa, 3.47, -0.1304, and -0.51, according to the previously reported data [30, 31], respectively. In these figures, the smallest cycle number (N) of the U-type module is about 41686, which is 32% larger than that of traditional unileg module. Moreover, due to the special structure of U-type unileg module, the damage of local position will not cause device failure. As for traditional unileg module, the module will stop working when the electrode is damaged. All in all, the low stress and high cycle lifetime show the high stability and commercial value of the U-type unileg thermoelectric modules.

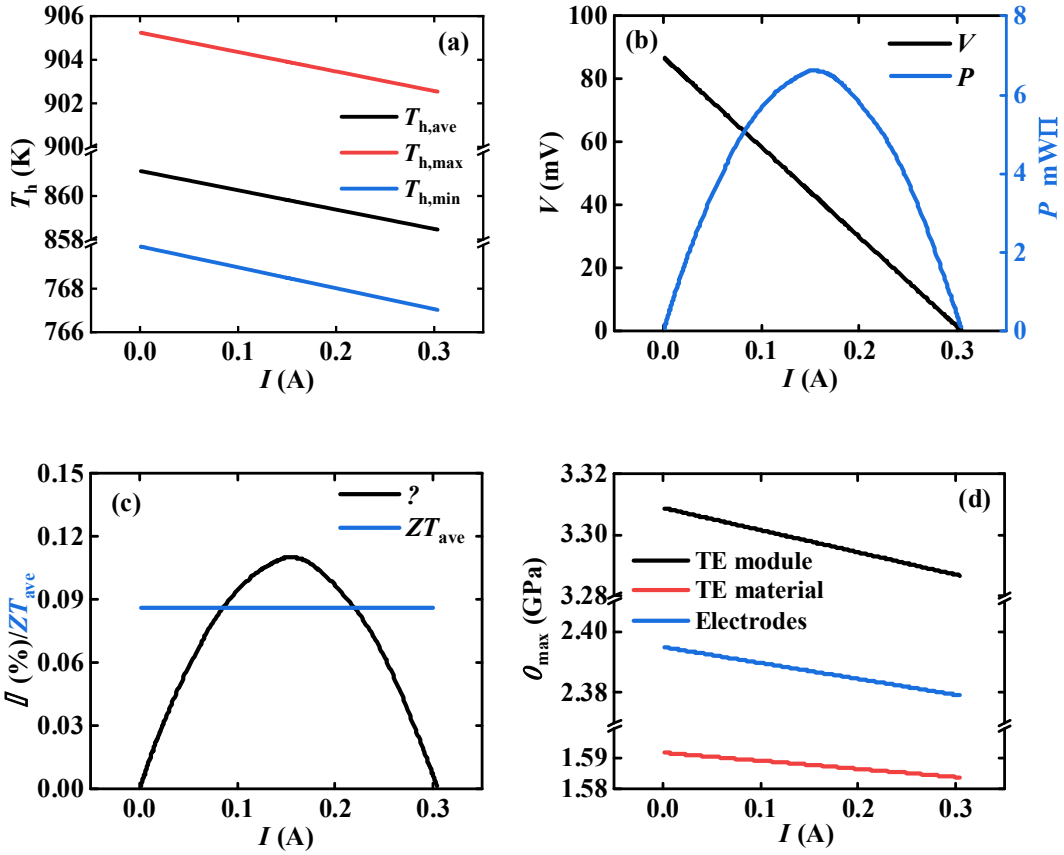

Figure 5 (a) average, maximum, and minimum hot-side temperature; (b) output voltage, and output power; (c) conversion efficiency, and average figure of merit; and (d) maximum von Mises stress for the U-type unileg thermoelectric module, thermoelectric material, and electrodes, as a function of current.

Table 1 Materials, couples number, temperature difference, output power and output power density for reported oxide-based modules.

Ref	p/n-type leg	N	ΔT(K)	P_{max}(mW)	p_{max}(mW/cm^2)
Lemonnier et al.	$Ca_{0.95}Sm_{0.05}MnO_3$	2	360	16	3.53
Conze et al.	TiO_x	20	500	120	13.3
Sharma et al.	$Ca_{0.92}La_{0.08}MnO_3$	9	480	50	12.5
This work	$Ca_{0.9}Dy_{0.1}MnO_3$	3	560	6.6	17.37

Thermoelectric modules as power generators are always used to supply electricity to applications in the loop, thus their output and mechanical performance are studied in a closed circuit. **Figure 5** presents the evolution of T_h, V, P, η and σ_{max} as I increases under closed-circuit conditions, when Q_h, and T_c are 6W, and 300K, respectively. In

Figure 5(a), it can be observed that $T_{h,ave}$, $T_{h,max}$, and $T_{h,min}$ decreased by about 3K with the increasing of I. This evolution is due to the coupled impact of Peltier effect and Joule heating. Based on the monotonically decreased temperature, V is linearly reduced as I enhances. The V-I linear curve follows the ohm`s law, which proves the correctness of these simulative results. Then, P is firstly enhanced as I enlarges and then reverses at I=0.15A. The P_{max}, 6.6mW, is obtained at load matching conditions. Compared to previous works about oxide-based unileg modules, as shown in **Table 1**, the U-type thermoelectric module shows a relatively higher electrical performance (P_{max}=17.37mW/cm^2). As for η, it firstly increases and then decreases with the increasing of I. The maximum value is only 0.11%, which is far from meeting the industrial requirements. The low η_{max} is mainly due to two reasons: low ZT_{ave} of n-type $CaMnO_3$-based thermoelectric material (only 0.086), and much unnecessary energy losses caused by Ag-coated right legs and contact resistances. **Figure 5(d)** shows that $\sigma_{max,TEM}$ drops from 3.31 to 3.29GPa when I varies from 0 to 0.3A, while $\sigma_{max,TE}$ is reduced from 1.59 to 1.58GPa. This stress reduction can be explained by the observed decrease of temperature.

In short, in the U-type unileg structure, one of the legs is practically short-circuited by the Ag-coating layer and acts as an electrical conductor in the structure, avoiding the damage of thermoelectric modules owing to the CTE difference between different components. Moreover, the structure eliminates the need for electrodes at the hot end of the thermoelectric legs, leading to higher stability and promising commercial value.

4. The effect of the radius of round corners

As observed in the previous results, the novel U-type unileg structure is beneficial for relieving stress intensity and enhancing mechanical properties; however, it is found that sharp change in local structural configuration also results in heavy stress concentration. Thus, in order to minimize stress and enlarge lifespan, round chamfering has been considered, and presented in **Figure 6(a)**. In this figure, r_u, and r_l are the fillet radius of upper and lower corners, respectively. **Figures 6(b)** and **6(c)** display the temperature and voltage distributions of the U-type unileg module with

r_u=1mm and r_l=0.5mm, under open-circuit conditions, at Q_h=6W and T_c=300K. Compared to the initial structure, the module has similar temperature and voltage distributions. However, due to the enlarged R_{th}, the improved U-type module with round chamfering has larger $T_{h,max}$ (965K) and, consequently, a slightly higher open-circuit voltage (91.9mV).

Figure 7 exhibits the $\sigma_{max,TEM}$, $\sigma_{max,TE}$, and $\sigma_{max,E}$ for the U-type unileg thermoelectric module, as a function of r_l, and r_u, at Q_h=6W and T_c=300K, under load matching conditions. As it can be seen in **Figure 7(a)**, with the enlarging of r_u, $\sigma_{max,TEM}$ firstly drops and then rises at r_l=0-0.3mm; the lowest point is obtained at r_u=0.1mm. At r_l=0.3-0.5mm, $\sigma_{max,TEM}$ shows a monotonously increasing tendency as r_u enlarges. With the increasing of r_l, the $\sigma_{max,TEM}$ is reduced and then enhanced at r_u=0mm and, additionally, the value keeps growing for r_u>0mm. The minimum value, 3.07GPa, is obtained at (r_u,r_l)=(0.1,0).

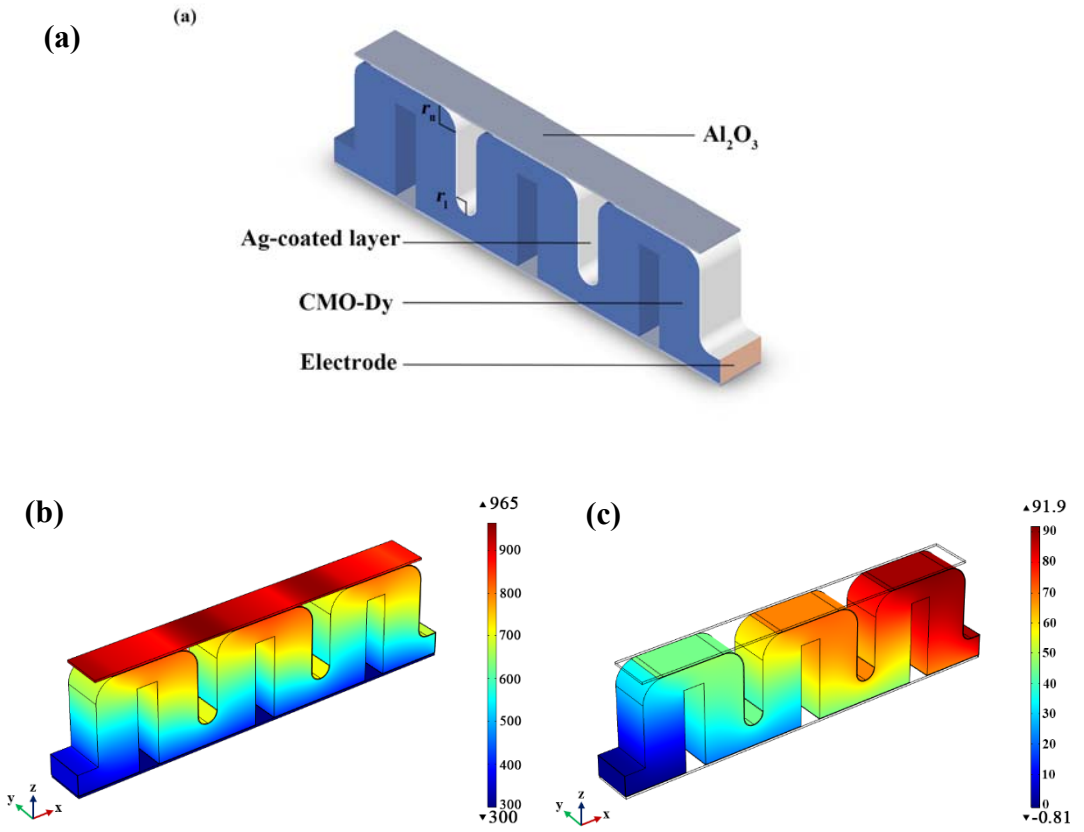

Figure 6 (a) Schematics of a novel U-type unileg thermoelectric module with rounded corners;(b) temperature; and (c) voltage distribution in the U-type unileg module under open-circuit conditions, when Q_h=6W and T_c=300K.

The evolution of $\sigma_{max,E}$, and $\sigma_{max,TE}$, is similar to the observed for $\sigma_{max,TEM}$, reaching the lowest values at (0,0.1), and (0,0.2), respectively. This abnormal evolution is due to fact that $\sigma_{max,TEM}$ is obtained at the upper corner position, with low r_u and r_l, as presented in **Figure 8(a)**. When increasing r_u and r_l, the $\sigma_{max,TEM}$ position is shifted to the bottom corner, as described in **Figure 8(b)**. In fact, the larger radius will result in lower concentrated stresses. For the upper corner (x=5mm), as shown in **Figure 9**, the local stress is rapidly and monotonously reduced from 3.31 to 2.05GPa, when r_u varies from 0 to 1mm. For the lower corner in **Figure 10**, the larger r_l alleviates the peak thermal stress intensity and shifts the high thermal stress region from the side to the center of the modules. Summarizing, the local stresses of upper and lower corners are effectively decreased by 38% and 45%, respectively, through adding rounded corners. However, for the whole U-type $CaMnO_3$ unileg module, the lowest stress (3.07GPa) is achieved at relatively low r_u (0.1mm), and r_l (0mm) values.

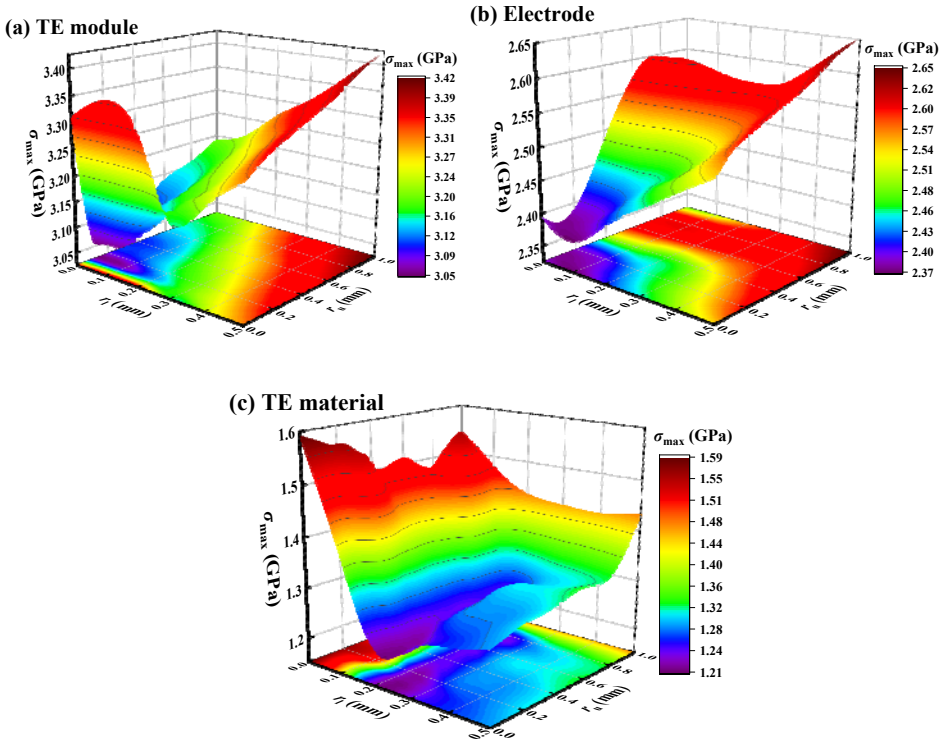

Figure 7 The maximum von Mises stress in (a) TE module; (b) electrode; and (c) TE material for the U-type unileg thermoelectric module as a function of the lower (r_l) and upper (r_u) radii, under load matching conditions.

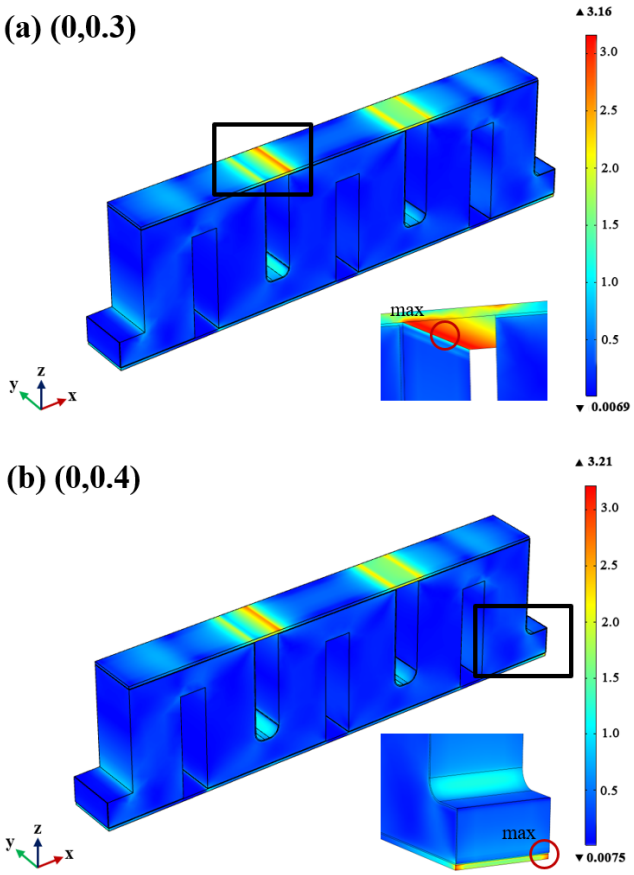

Figure 8 The distribution of von Mises stress for the U-type unileg module at (a) (r_u,r_l)=(0,0.3); and (b) (0,0.4).

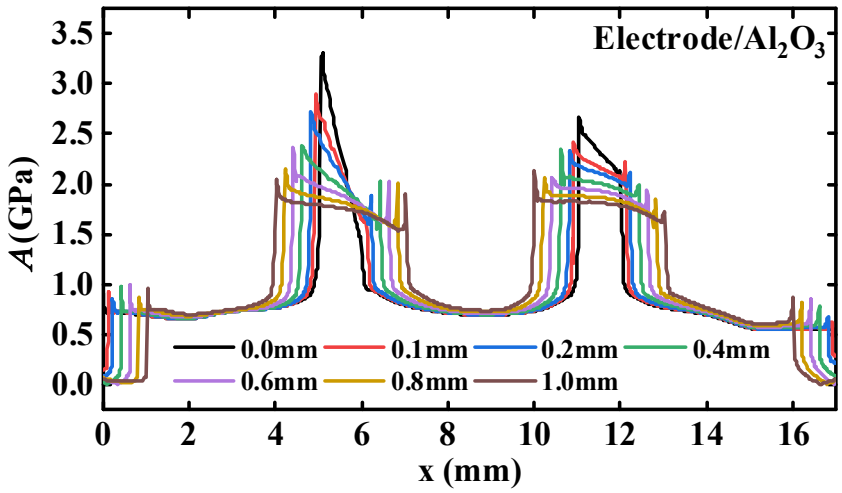

Figure 9 The variation of von Mises stress for the electrode/Al_2O_3 interface along x-axis at different upper radii.

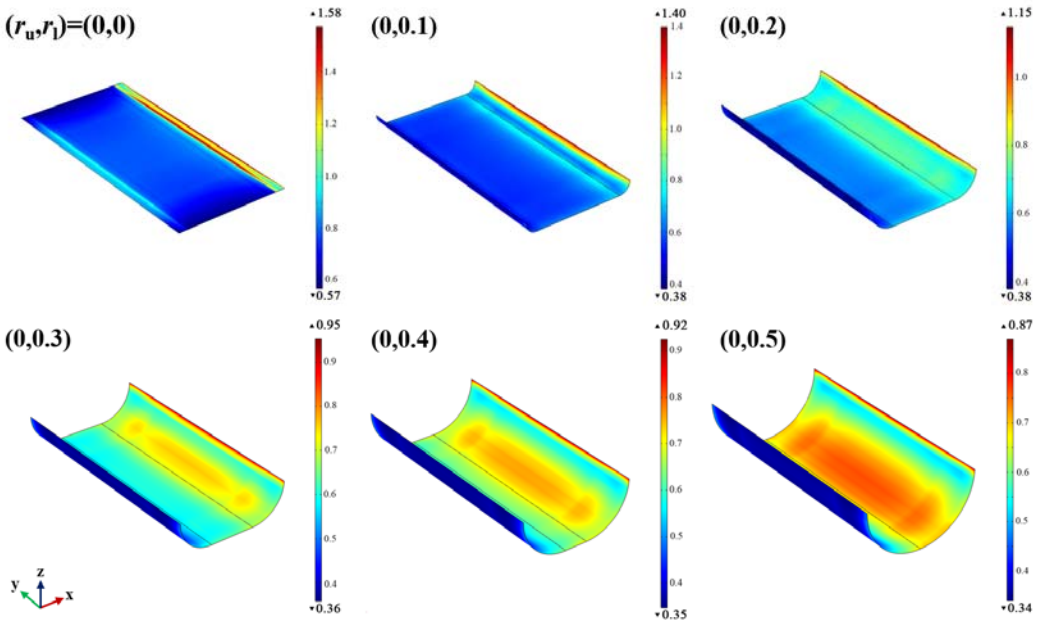

Figure 10 The distribution of von Mises stress for the first lower corner at different lower radii.

Figure 11 displays the $T_{h,ave}$, average temperature of the first lower corner ($T_{l,ave}$), V_o, R_{in}, I, and P_{max} of the U-type unileg module as a function of r_u, and r_l, under load matching condition, while Q_h is 6W and T_c is 300K. The r_u changes in the range of 0 to 1mm, meanwhile, the r_l varies from 0 to 0.5mm. In **Figure 11(a)**, it can be observed that $T_{h,ave}$ monotonously enhances when r_u is larger due to the increased R_{th}, and fluctuates by about 1K with the increasing of r_l. Moreover, $T_{l,ave}$ decreases when r_u is enlarged, while it firstly decreases and then improves as r_l raises (see **Figure 11 (b)**). Consequently, the difference value between $T_{h,ave}$ and $T_{l,ave}$ at r_u=1mm is enlarged by about 55K compared to the value at r_u=0mm, meantime, the temperature difference is firstly declined and slightly enhanced around 5K as r_l increases.

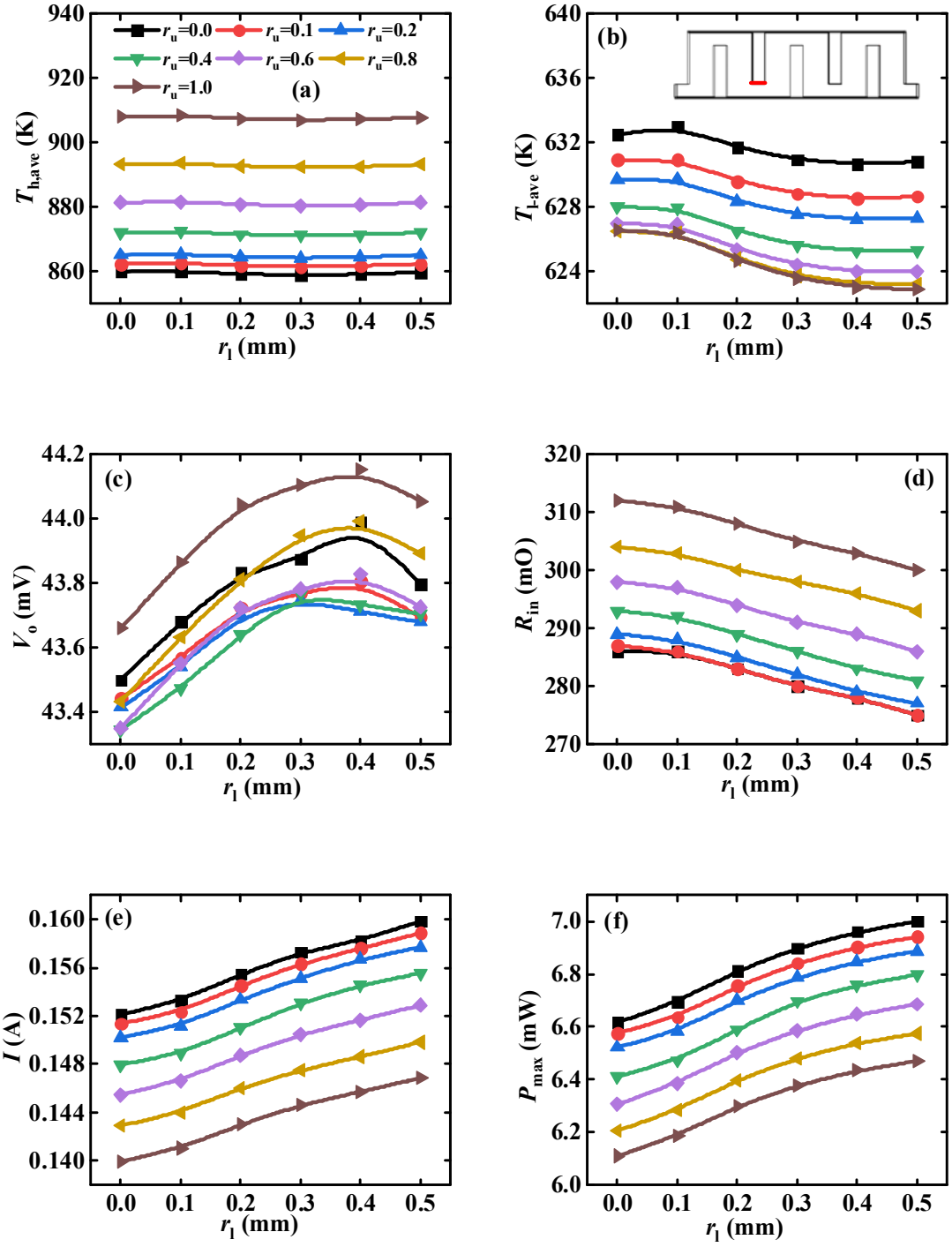

Figure 11 (a) Hot-side; and (b) lower corner average temperatures; (c) output voltage; (d) internal resistance; (e) working current; and (f) maximum output power, as a function of fillet radius of lower corner (r_l) at different fillet radii of upper corner (r_u), under load matching conditions.

Based on the temperature variation, as presented in **Figure 11 (c)**, V_o is firstly improved and then it is reduced with the increase of r_l and the decrease of r_u,

achieving the peak value (44.15mV) at r_u of 1mm, and r_l of 0.4mm. In addition, higher r_u and lower r_l lead to larger material resistance, thus the R_{in} enhances with increasing r_u and decreasing r_l, as shown in **Figure 11(d)**. Then, owing to the coupled effect of V_o and R_{in}, I diminishes when r_u increases and improves when r_l increases (see **Figure 11 (e)**). Therefore, the optimal P_{max} values are achieved at lower r_u and higher r_l. As described in **Figure 11(f)**, the maximum P_{max}, 7mW, is obtained at r_u=0mm, and r_l=0.5mm, which is 6% larger than that of the module with straight corners.

All in all, the local stress concentration and output performance are influenced by adding rounded corners. The local stress can be greatly decreased at larger r_u and r_l, while power output is enhanced at lower r_u and higher r_l. However, the structure modification results in the transfer of maximum stress position, and the lowest $\sigma_{max,TEM}$, obtained at (r_u, r_l)=(0.1, 0), is only 7% lower than the obtained for the initial structure. Therefore, in order to reduce the $\sigma_{max,TEM}$, more geometric parameters, besides local structure, need to be systematically optimized.

5. The influence of geometric size

As above mentioned, geometric size is an essential factor for the location of the maximum stress and the level of thermal stress intensity. For the U-type unileg structured module, the Ag-coated right leg as conductive wire has a more complex structure, which has great influence on module output and mechanical performance. Hence, in this section, the influence of right leg length (L_R), and Ag-coating layer thickness (H_{Ag}), as the two most important geometric factors, on the performance and stress distribution of the optimal U-type thermoelectric module, with r_u=0.1mm and r_l=0mm, is investigated at Q_h=6W and T_c=300K.

Figure 12 presents $\sigma_{TEU/E}$, $\sigma_{E/A}$, and σ_A along the x-axis direction at different L_R under load matching conditions. The curves evolution along x-axis is roughly similar for different L_R values. The high stress occurs locally at the edge of thermoelectric unilegs, such as x=5, 6, 11, and 12mm, and the stress becomes more moderate at simple structural parts. However, the stress in different regions shows various

changing trends as L_R varies. In the unileg region, the stress value is decreased when L_R is larger due to the lower temperature achieved. In the junction region, the stress is enhanced at larger L_R, as shown in **Figures 12(b)** and **12(c)**. Moreover, the local range of stress variation is also diverse due to the structural changes. Taking the region 1 in **Figure 12(a)** as an example, $\sigma_{TEU/E}$ firstly reaches the lowest point and then increases as x increases for the different L_R. The position with the lowest point gradually shifts to smaller x with the increase of L_R, which agrees well with the modified geometric structure. Then, at x=16.33-16.64mm local position, the maximum $\sigma_{TEU/E}$ is obtained for L_R=1.0mm, which is nor the largest or smallest L_R. As for σ_A in region 1, the value firstly declines, later rises and, finally, declines again.

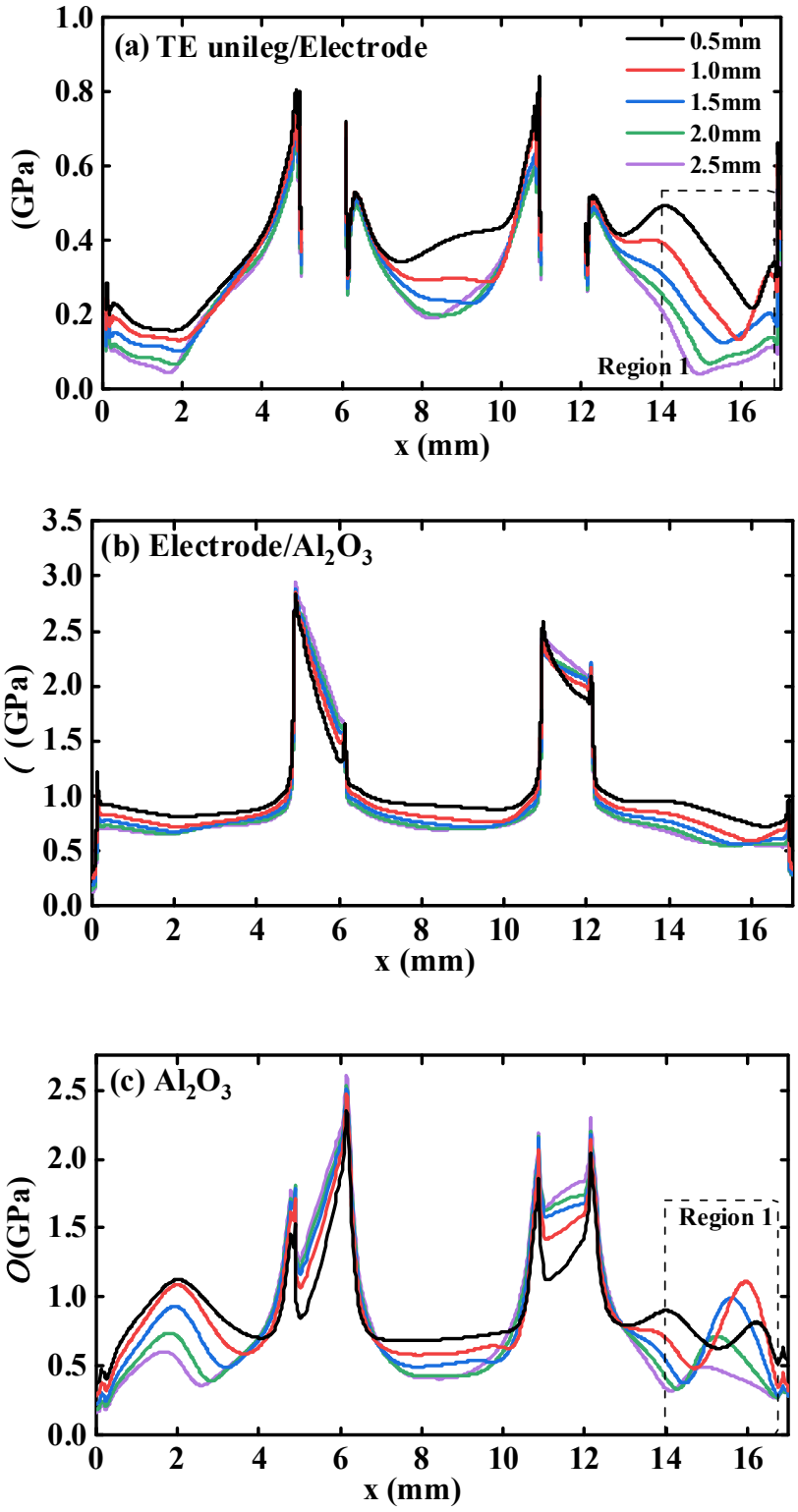

Figure 12 Von Mises stress of (a) thermoelectric unileg/electrode interface; (b) electrode/Al_2O_3 interface; and (c) Al_2O_3 surface along x-axis, with different right legs length, under load matching conditions.

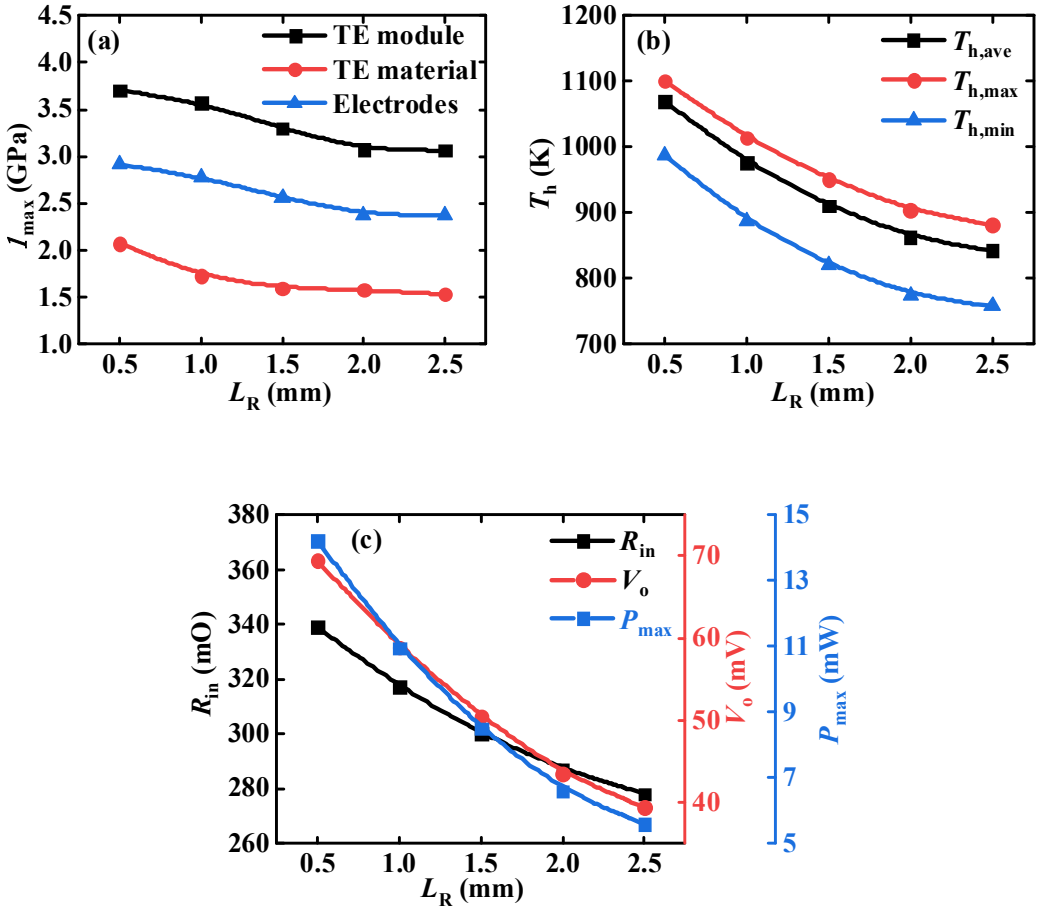

Figure 13 (a) Maximum von Mises stress of thermoelectric module, thermoelectric material, and electrodes; (b) average, maximum, and minimum hot-side temperature; (c) working current, output voltage, and maximum output power for the U-type thermoelectric unileg module with r_u=0.1mm, and r_l=0mm, as a function of right legs length, under load matching conditions.

Furthermore, the extreme point is achieved at a smaller x as L_R increases. In conclusion, as plotted in **Figure 13(a)**, σ_{max} of different components tends to decrease as the L_R increases from 0.5 to 2.5mm. The phenomenon can be reasoned taking into account two factors: On one hand, smaller L_R results in higher overall R_{th} per surface area and larger temperature gradient. On the other hand, rapid changes in local structure lead to stress concentration. Thus, in order to achieve higher mechanical performance, larger length of right legs should be chosen. **Figure 13(b) and 13(c)** present T_h, R_{in}, V_o, and P_{max} of the optimal U-type thermoelectric module, as a function of L_R. As it can be seen in the figure, the increase of L_R leads to decreasing

R_{in} due to the enlarged cross-sectional area. The variation tendency nearly fits with the results obtained through the equation of shunt resistance, R_{in}~$(1/(R_{left}^{-1}+kL_R))$, where R_{left} is resistance of left leg and k is a coefficient depending on geometric sizes and electrical resistivity. However, the increased L_R also results in a lower R_{th}, leading to smaller ΔT at a certain Q, as shown in **Figure 13(b)**, and, subsequently, diminished V_o. Moreover, V_o shows a more significant reduction compared to R_{in} and, consequently, P_{max} finally drops from 14.2 to 5.6mW when L_R increases from 0.5 to 2.5mm. In a word, the optimization strategies for mechanical and output performance are opposite. Greater L_R deteriorates the module performance, but it is still beneficial for mechanical properties by decreasing the peak thermal stress and dispersing the high thermal stress regions. Hence, after comprehensive consideration, the L_R of 1.5-2mm is considered as the optimal size because of the low gradient of σ_{max} at L_R>2mm.

The thickness of Ag-coating layer is another important factor that affects thermal stress distribution. **Figure 14** displays $\sigma_{TEU/E}$, $\sigma_{E/A}$, and σ_A along x-axis for different H_{Ag} values. For the local hot-side stress, the values are lower for larger H_{Ag} due to the induced decrease of T_h. To more comprehensively study the change rules, **Figure 15(a)** shows the relationhship between σ_{max} of different components and H_{Ag}. In this case, $\sigma_{max,TEM}$ is larger than $\sigma_{max,E}$, and $\sigma_{max,TE}$ at any H_{Ag} value, indicating that the maximum stress always occurs on the Al_2O_3 substrate. Moreover, the stress firstly decreases and then increases as H_{Ag} increases. The minmum point of $\sigma_{max,TEM}$, and $\sigma_{max,E}$ is achieved for H_{Ag}=35μm, while the lowest $\sigma_{max,TE}$ value is obtained for H_{Ag}=65μm. **Figures 15(b)** and **15(c)** depict T_h, R_{in}, V_o, and P_{max} of the optimal U-type thermoelectric module as a function of H_{Ag}, at Q_h=6W and T_c=300K, under load matching conditions. When H_{Ag} is increased from 20 to 80μm, R_{th} is reduced and, consequently, $T_{h,ave}$ is monotonously decreased from 902.4 to 821.3K. The decreased $T_{h,ave}$ causes, in turn, the reduction of V_o. Then, although R_{in} shows a downwards trend as H_{Ag} increases, P_{max} drops from 8.0 to 5.3mW when H_{Ag} is enhanced from 20 to 80μm. In conclusion, althrough the stress concentration at hot end is slightly severe, a relatively thinner Ag-coating layer of about 35μm is beneficial for relieving the overall stress and enhancing module performance simultaneously.

In brief, greater L_R results in worse module performance but better mechanical properties. Moreover, the optimal P_{max} and lowest $\sigma_{max,TEM}$ are all obatined with a relatively thin Ag-coating layer. Above results proved that different performance demands will be satisfied through the optimization of geometric size, however, the final design for any practical devices should be proposed after considering the actual performance requirements.

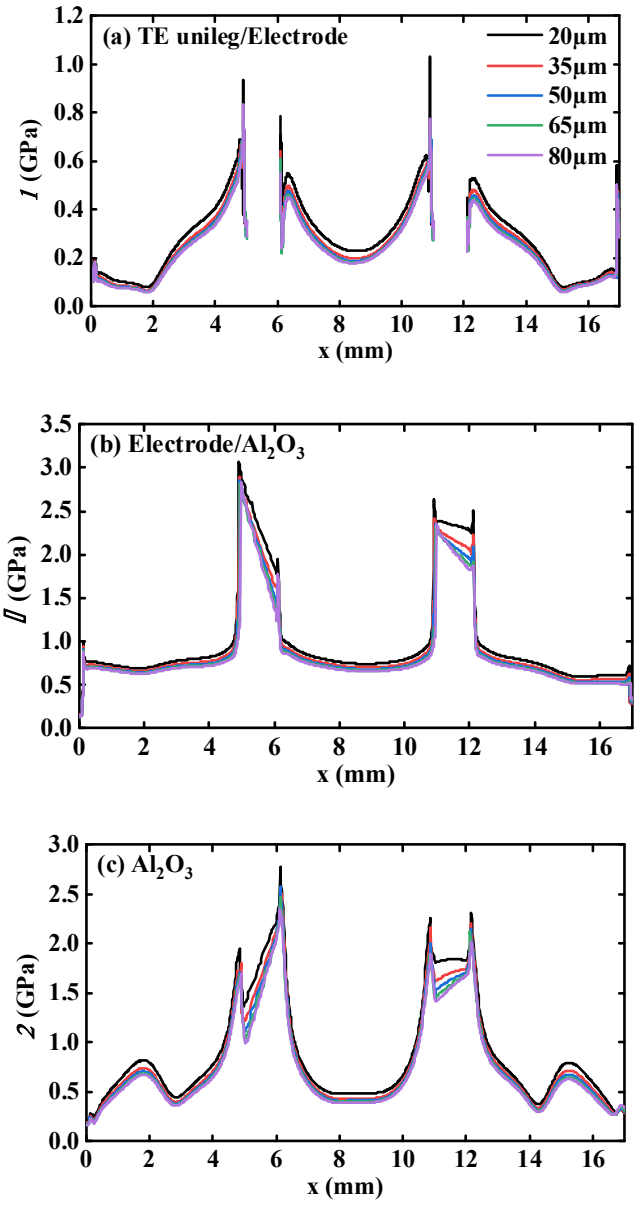

Figure 14 Von Mises stress of (a) thermoelectric unileg/electrode interface; (b) electrode/Al_2O_3 interface; and (c) Al_2O_3 surface along x-axis for different Ag layer thickness.

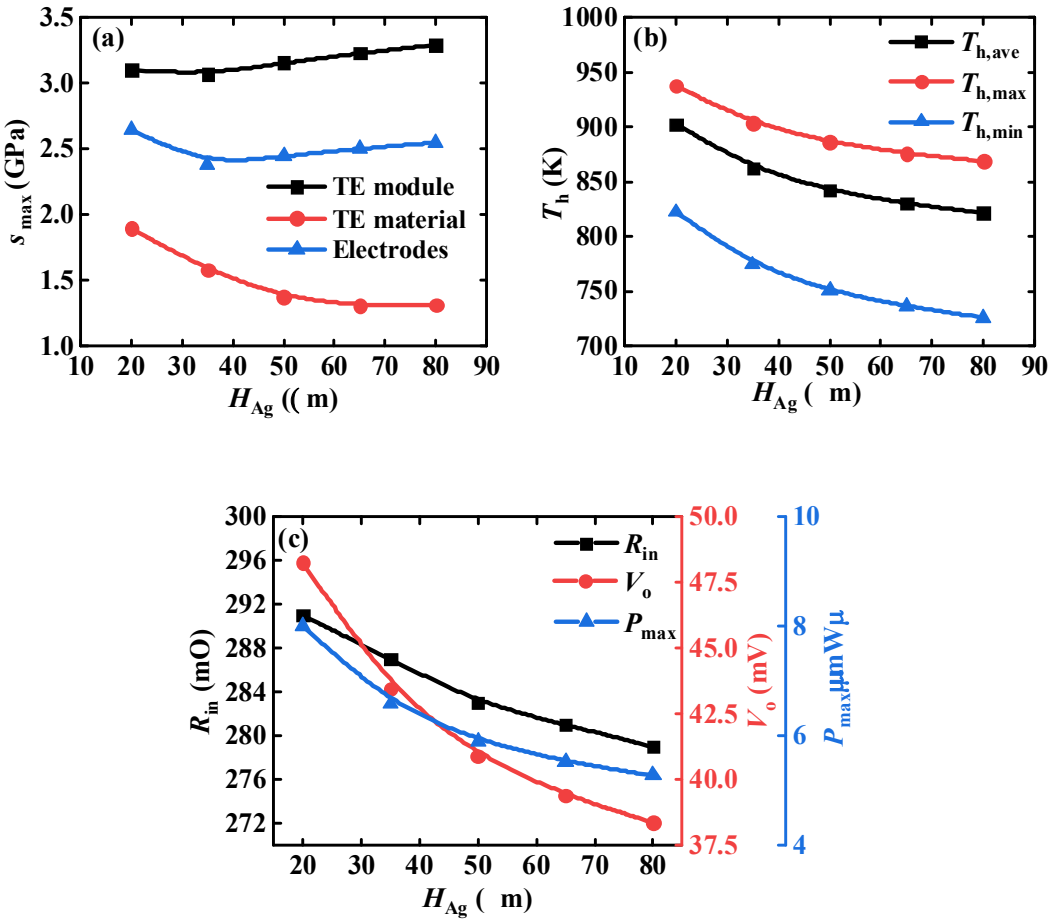

Figure 15 (a) Maximum von Mises stress of thermoelectric module, thermoelectric material, and electrodes; (b) average, maximum, and minimum hot-side temperature; and (c) working current, output voltage, and maximum output power for the U-type thermoelectric unileg module with r_u=0.1mm and r_l=0mm, as a function of Ag layer thickness, under load matching conditions.

6. Conclusion

A $CaMnO_3$-based U-type thermoelectric module combining unileg structure and pn-junction has been for the first time, in the best of our knowledge, proposed and investigated in this paper. In this structure, right leg is practically short-circuited through coating it with conductive material, acting as an electrical conductor for the unileg structure. The proposed structure avoids the module failure due to high thermal stress, produced at its hot side, between the thermoelectric materials and the electrode. Moreover, the need for soldering at the hot end of the thermoelectric unilegs is eliminated, and the module can keep working even if the hot-side electrode is broken.

The U-type unileg module can achieve P_{max} of 6.6mW, σ_{max} of 3.31GPa and N of 41686 cycles at Q_h=6W and T_c=300K. The σ_{max} and N are 46% and 132% of those obtained in traditional unileg modules with the same material and module size, indicating its high thermal stability. Based on the structural modifications performed to decrease the thermal stresses, the effect of r_u and r_l has been investigated. The results showed that lower r_u and higher r_l are beneficial for improving power output. On the other hand, larger r_u and r_l are suitable to relieve the local stress concentration; however, the lowest stress of overall module has been obtained for r_u=0.1mm, and r_l=0mm. Envisaging further decreasing the stress and improving module performance, the effect of L_R and H_{Ag} has also been considered. The results showed that greater L_R deteriorates the module performance, but it is beneficial for mechanical properties by decreasing the peak stress and dispersing the high thermal stress regions. Moreover, a relatively thin Ag-coating layer (35μm) is suitable for obtaining high P_{max} and relieving $\sigma_{max,TEM}$ simultanously. To summarize, the U-type thermoelectric module has shown to have high thermal and mechanical stability under high temperatures and thermal cycling conditions, which would be highly beneficial for commercializing high-temperature thermoelectric devices with excellent mechanical strength and long lifespan.

Declaration of interests

There are no conflicts to declare.

Credit authorship contribution statement

Xue Wang: Conceptualization, Data curation, Investigation, Formal analysis, Visualization, Writing-Original draft preparation. **Hongchao Wang:** Supervision, Project administration, Writing-Reviewing and Editing. **Wenbing Su:** Resources. **Tingting Chen:** Software. **Chang Tan:** Validation. **M. A. Madre:** Validation. **A. Sotelo:** Conceptualization, Writing-Reviewing and Editing. **Chunlei Wang:** Supervision.

Acknowledgements

The work is financially supported by National Key R&D Program of China of 2017YFE0195200, the Natural Science Fund of China under grant Nos. 51871134, 51672159, 5201101703, the Science Fund of Shandong Province under grant No. ZR2019MEM007, and Qilu Young Scholar Program of Shandong University. M. A. Madre, and A. Sotelo also acknowledge the MINECO-FEDER (MAT2017-82183-C3-1-R) and Gobierno de Aragón-FEDER (Research Group T54-20R) for funding.

Nomenclature:

TEG: thermoelectric power generator

T: temperature (K)

ΔT: temperature difference (K)

ρ_d: density (kg/m^3)

E: Young's modulus (GPa)

v: Poisson's rate

CTE: coefficient of thermal expansion (10^{-6}/K)

S: Seebeck coefficient (V/K)

ρ: electrical resistivity (Ωm)

κ: thermal conductivity (W/mK)

P_c: Peltier coefficient (V)

C_p: heat capacity (J/kgK)

R_{in}: inner resistance (Ω)

R_L: load resistance (Ω)

V: output voltage (V)

V_{oc}: open-circuit voltage (V)

I: working current (A)

P: output power (W)

Q_h: absorbed heat in the hot side (W)

η: conversion efficiency

σ: von Mises stress (GPa)

N: number of full cycles to failure

N_f: number of load reversals

r_u: fillet radius of upper corners (mm)

r_l: fillet radius of lower corners (mm)

H_{Ag}: Ag layer thickness (μm)

L_R: length of right legs (mm)

Subscripts:

$_{h}$: hot side

$_{c}$: cold side

$_{ave}$: average value

$_{max}$: maximum value

$_{min}$: minimum value

$_{a}$: actual

$_{r}$: reverse

$_{TEM}$: Thermoelectric module

$_{TE}$: Thermoelectric material

$_{E}$: Electrodes

$_{A}$: upper surface of Al_2O_3 substrate

$_{TEU/E}$: thermoelectric unileg/electrode interface

$_{E/A}$: electrode/Al_2O_3 interface

References:

[1] He J, Tritt TM. Advances in thermoelectric materials research: Looking back and moving forward. Science 2017;357:eaak9997.

[2] Bahrami A, Schierning G, Nielsch K. Waste recycling in thermoelectric materials. Adv Energy Mater 2020;10:1904159.

[3] Zeb K, Ali SM, Khan B, Mehmood CA, Tareen N, Din W, et al. A survey on waste heat recovery: Electric power generation and potential prospects within Pakistan. Renew Sust Energ Rev 2017;75:1142-1155.

[4] Liu WS, Jie Q, Kim HS, Ren ZF. Current progress and future challenges in thermoelectric power generation: From materials to devices. Acta Mater 2015;87:357-376.

[5] Dargusch M, Liu WD, Chen ZG. Thermoelectric generators: alternative power supply for wearable electrocardiographic systems. Adv Sci 2020;18:2001362.

[6] Nozariasbmarz A, Collins H, Dsouza K, Polash MH, Hosseini M, Hyland M, et al. Review of wearable thermoelectric energy harvesting: From body temperature to electronic systems. Appl Energ 2020;258:114069.

[7] Hong S, Gu Y, Seo JK, Wang J, Liu P, Meng YS, et al. Wearable thermoelectrics for personalized thermoregulation. Sci Adv 2019;5:eaaw0536.

[8] Kütt L, Millar J, Karttunen A, Lehtonen M, Karppinen M. Thermoelectric applications for energy harvesting in domestic applications and micro-production units. Part I: Thermoelectric concepts, domestic boilers and biomass stoves. Renew Sust Energ Rev 2018;98:519-544.

[9] Clin T, Turenne S, Vasilevskiy D, Masut RA. Numerical simulation of the thermomechanical behavior of extruded bismuth telluride alloy module. J Electron Mater 2009;38:994-1001.

[10] Chavez R, Angst S, Hall J, Maculewicz F, Stoetzel J, Wiggers H, et al. Efficient p-n junction-based thermoelectric generator that can operate at extreme temperature conditions. J Phys D Appl Phys 2018;51:014005.

[11] Lemonnier S, Goupil C, Noudem J, Guilmeau E. Four-leg $Ca_{0.95}Sm_{0.05}MnO_3$ unileg thermoelectric device. J Appl Phys 2008;104:014505.

[12] Wijesekara W, Rosendahl L, Brown DR, Snyder GJ. Unileg thermoelectric generator design for oxide thermoelectrics and generalization of the unileg design using an idealized metal. J Electron Mater 2014;44:1834-1845.

[13] García G, Martínez-Filgueira P, Cordon M, Urrutibeascoa I, Sotelo A, Diez JC, et al. Π unileg thermoelectric structure for cycling robustness at high temperature and low manufacturing cost. J Electron Mater 2019;48:2010-2017.

[14] Erturun U, Erermis K, Mossi K. Influence of leg sizing and spacing on power generation and thermal stresses of thermoelectric devices. Appl Energ 2015;159:19-27.

[15] Erturun U, Erermis K, Mossi K. Effect of various leg geometries on thermo-mechanical and power generation performance of thermoelectric devices. Appl Therm Eng 2014;73:128-141.

[16] Al-Merbati AS, Yilbas BS, Sahin AZ. Thermodynamics and thermal stress analysis of thermoelectric power generator: Influence of pin geometry on device performance. Appl Therm Eng 2013;50:683-692.

[17] Yilbas BS, Akhtar SS, Sahin AZ. Thermal and stress analyses in thermoelectric generator with tapered and rectangular pin configurations. Energy 2016;114:52-63.

[18] Wang RC, Meng ZH, Luo D, Yu W, Zhou WQ. A comprehensive study on X-type thermoelectric generator modules. J Electron Mater 2020;49:4343-4354.

[19] Wu YJ, Ming TZ, Li XH, Pan T, Peng K, Luo XY. Numerical simulations on the temperature gradient and thermal stress of a thermoelectric power generator. Energ Convers Manage 2014;88:915-927.

[20] Wang X, Wang HC, Su WB, Wang T, Madre MA, Zhai JZ, et al. A novel multilayer composite structured thermoelectric module with high output power. J Mater Chem A 2020;8:3379.

[21] Wang X, Wang HC, Su WB, Mehmood F, Zhai JZ, Wang T, et al. Geometric structural design for lead tellurium thermoelectric power generation application. Renew Energ 2019;141:88-95.

[22] Shittu S, Li GQ, Zhao XD, Ma XL, Akhlaghi YG, Ayodele E. High performance and thermal stress analysis of a segmented annular thermoelectric generator. Energ Convers Manage 2019;184:180-193.

[23] Park K, Lee GW. Fabrication and thermoelectric power of π-shaped $Ca_3Co_4O_9$/$CaMnO_3$ modules for renewable energy conversion. Energy 2013;60:87-93.

[24] Wang T, Nan PF, Wang HC, Su W,B Sotelo A, Zhai JZ, et al. Right heterogeneous microstructure for achieving excellent thermoelectric performance in $Ca_{0.9}R_{0.1}MnO_{3-\delta}$ (δ = Dy, Yb) ceramics. Inorg Chem 2018;57:9133-9141.

[25] Wang X, Wang HC, Su WB, Zhai JZ, Wang T, Chen TT, et al. Optimization of the performance of the SnTe uni-leg thermoelectric module via metallized layers. Renew Energ 2019;131:606-616.

[26] Arai K, Matsubara M, Sawada Y, Sakamoto T, Kineri T, Kogo Y, et al. Improvement of electrical contact between TE material and Ni electrode interfaces by application of a buffer layer. J Electron Mater 2012;41:1771-1777.

[27] Antonova EE, Looman DC. Finite elements for thermoelectric device analysis in ANSYS. 2005 International Conference on Thermoelectrics, 2005.

[28] Bejan A, Kraus A. Heat Transfer Handbook. Wiley, New York, 2003.

[29] Ibeagwu OI. Modelling and comprehensive analysis of TEGs with diverse variable leg geometry. Energy 2019;180:90-106.

[30] Quintero P, McCluskey P, Koene B. Thermomechanical reliability of a silver nano-colloid die attach for high temperature applications. Microelectron Reliab 2014;54:220-225.

[31] Chen G, Yu L, Mei YH, Li X, Chen X, Lu GQ. Uniaxial ratcheting behavior of sintered nanosilver joint for electronic packaging. Mater Sci Eng A 2014;591:121-129.

[32] Heckel TK, Christ HJ. Thermomechanical fatigue of the TiAl intermetallic alloy TNB-V_2. Exp Mech 2009;50:717-724.

[33] Tomeš P, Robert R, Trottmann M, Bocher L, Aguirre MH, Bitschi A, et al. Synthesis and characterization of new ceramic thermoelectrics implemented in a thermoelectric oxide module. J Electron Mater 2010;39:1696-1703.

[34] Karri NK, Mo C. Reliable thermoelectric module design under opposing requirements from structural and thermoelectric considerations. J Electron Mater 2017;47:3127-3135.

Electronic Supplementary Information

U-type Unileg Thermoelectric Module: A Novel Structure for High-temperature Application with Long Lifespan

Xue Wang[1], Hongchao Wang[*,1], Wenbing Su[1], Tingting Chen[1], Chang Tan[1], M. A. Madre[2], A. Sotelo[§,2], Chunlei Wang[#,1]

[1]School of Physics, State Key Laboratory of Crystal Materials, Shandong University Jinan 250100, P. R. China

[2]INMA, Aragon Institute of Nanoscience and Materials (CSIC-Universidad de Zaragoza), María de Luna, 3. 50018 Zaragoza, Spain

[*] E-mail: wanghc@sdu.edu.cn (H. Wang)

[§] E-mail: asotelo@unizar.es (A. Sotelo)

[#] E-mail: wangcl@sdu.edu.cn (C. Wang)

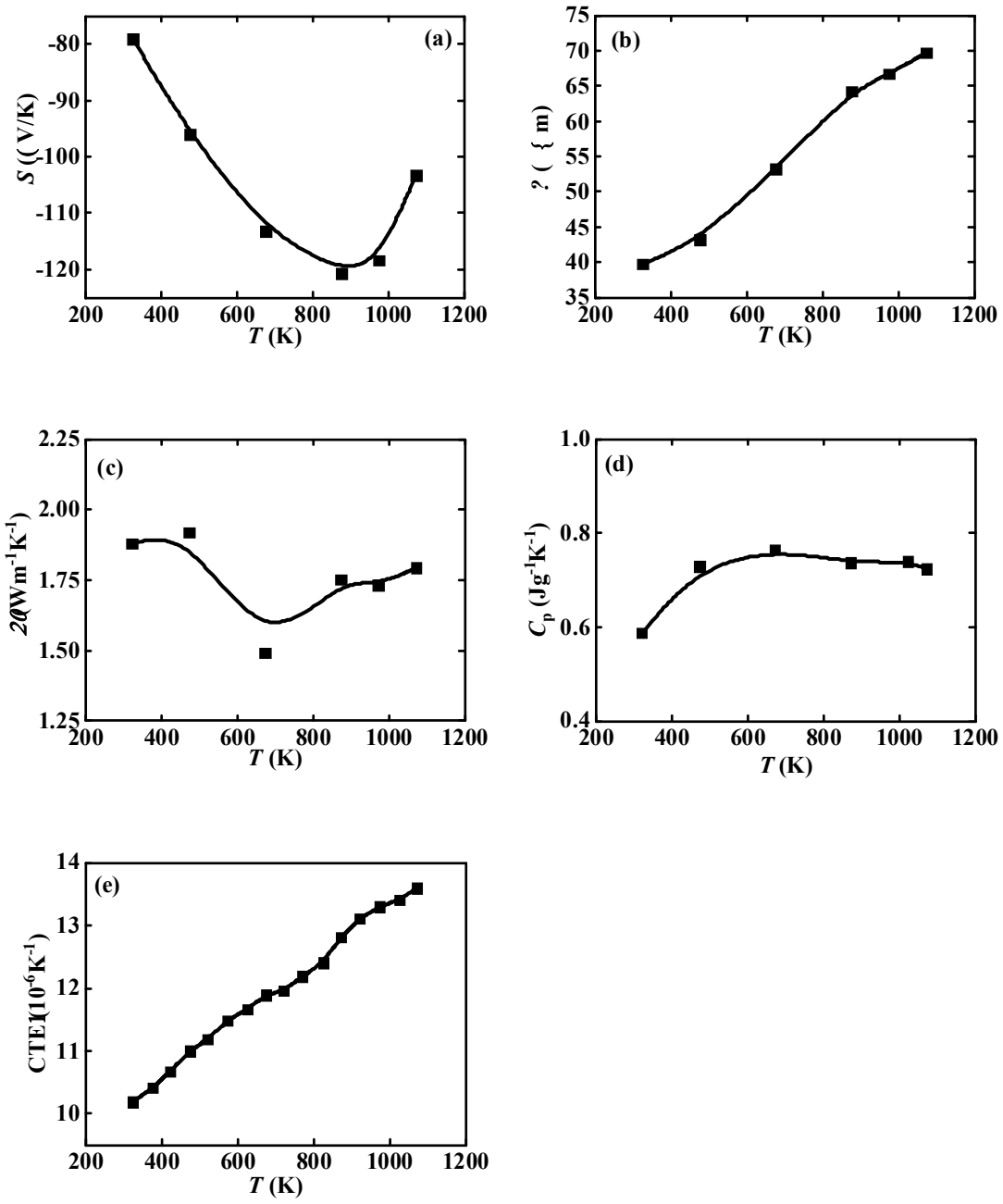

Figure S1 (a) Seebeck coefficient; (b) electric resistivity; (c) thermal conductivity; (d) heat capacity; and (e) thermal expansion coefficient of Dy-doped $CaMnO_3$.

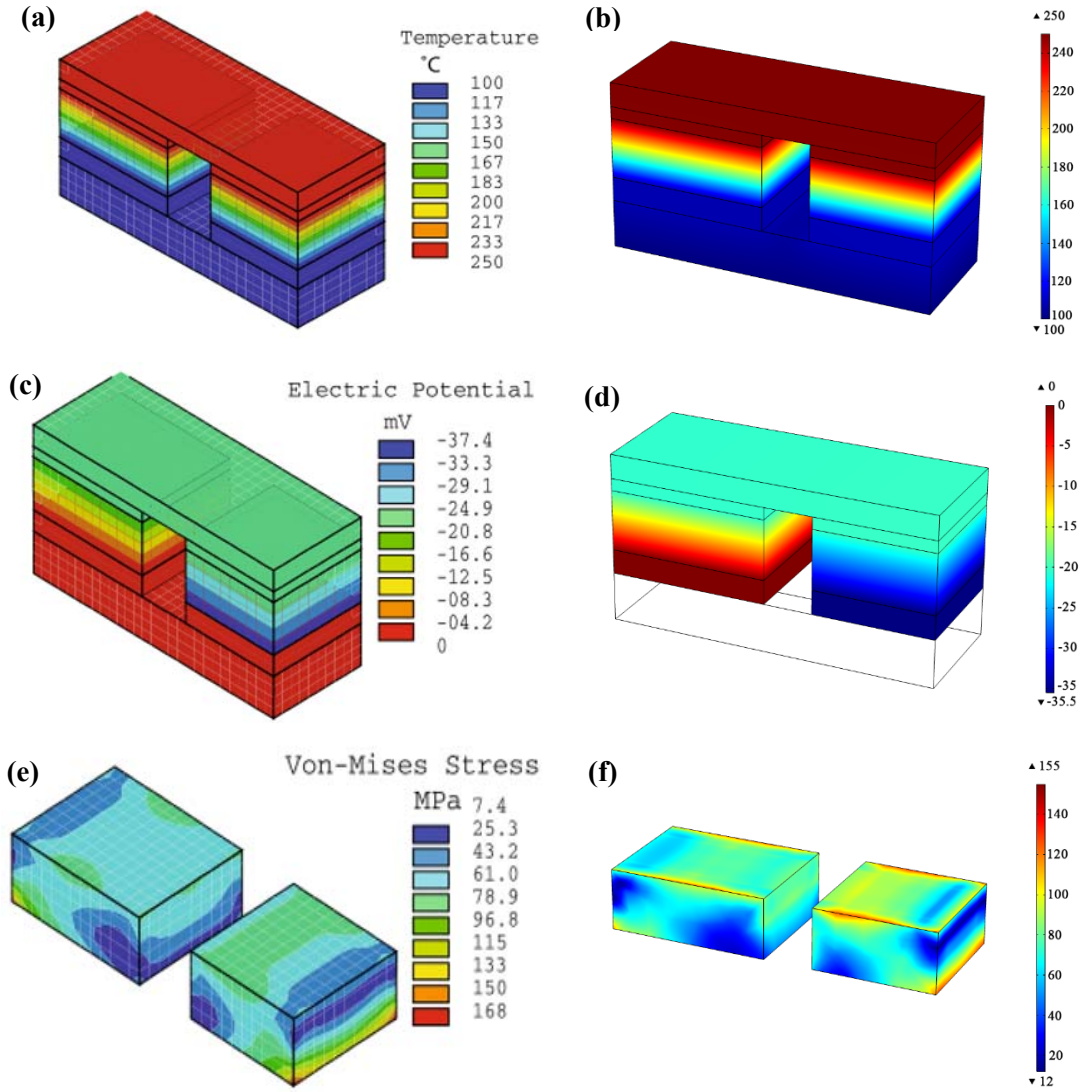

Figure S2 Validation of present simulations with previous study. Distributions of (a) (b) temperature; (c) (d) voltage; and (e) (f) von Mises stress.

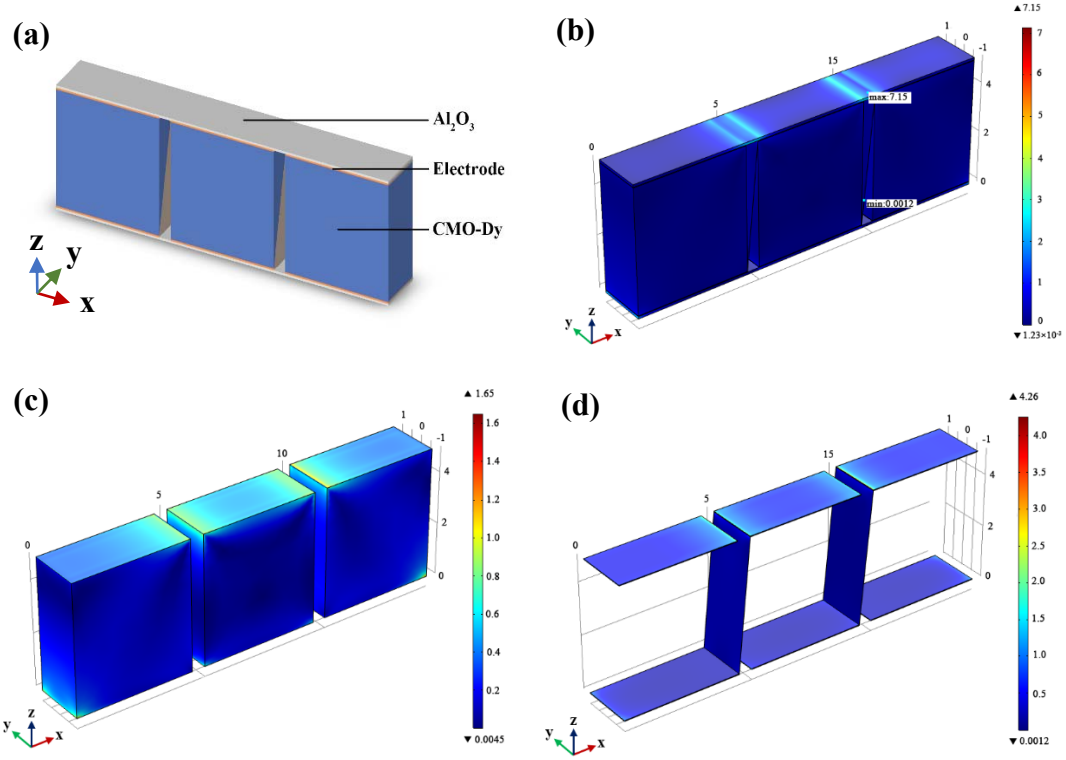

Figure S3 (a) Schematics of traditional unileg modules. The von Mises stress distributions in (b) traditional unileg module; (c) thermoelectric leg; and (d) electrode under open-circuit conditions.

Table S1 Properties of CMO-Dy, Ag and Al_2O_3.

Material	**CMO-Dy**	**Ag**	**Al_2O_3**
ρ (kg/m^3)	$\rho(T)$	10500	3965
***E* (GPa)**	142	83	350
v	0.3	0.37	0.3
CTE (10^{-6}/K)	$CTE(T)$	18.9	8.8
C_p (J/kgK)	$C_p(T)$	235	730
***k* (W/mK)**	$k(T)$	429	35